Thin Solid Films xxx (2009) xxx–xxx

Contents lists available at ScienceDirect

Thin Solid Films

journal homepage: www.elsevier.com/locate/tsf

The adhesive properties of pyridine-terminated self-assembled monolayers

James Bowen [a], Mayandithevar Manickam [a], Parvez Iqbal [a], Stephen D. Evans [b], Kevin Critchley [b], Jon A. Preece [a], Kevin Kendall [c,*]

[a] School of Chemistry, The University of Birmingham, Edgbaston, Birmingham, B15 2TT, United Kingdom
[b] Department of Physics and Astronomy, The University of Leeds, Woodhouse Lane, Leeds, LS2 9JT, United Kingdom
[c] School of Chemical Engineering, The University of Birmingham, Edgbaston, Birmingham, B15 2TT, United Kingdom

ARTICLE INFO

Article history:
Received 12 August 2008
Received in revised form 19 January 2009
Accepted 22 January 2009
Available online xxxx

Keywords:
Self-assembled monolayer
Adhesion
Surface chemistry
Pyridine
Gold
Atomic force microscopy

ABSTRACT

The atomic force microscopy (AFM) adhesion force behaviour and contact angle titration behaviour of self-assembled monolayers (SAMs) presenting surface pyridine and substituted pyridine moieties has been investigated as a function of pH and electrolyte concentration. The pK_as of the pyridine moieties were modified through the incorporation of fluorine, chlorine and bromine substituents in the pyridyl ring. Contact angle titration and AFM adhesion force measurements were performed using aqueous phosphate buffered saline solutions over the pH range 3–9, and at concentrations of 150 mM and 0.1 mM. AFM adhesion force measurements were performed using a clean Si_3N_4 pyramidal-tipped AFM cantilever.

1. Introduction

Since it was invented by Binnig, Quate and Gerber [1] the atomic force microscope (AFM) has been used to analyse the interactions which exist between surfaces of interest. The AFM has provided the modern researcher with the ability to perform repeated, accurate force measurements between a probe and a surface [2]. The data obtained has been used in the research and development of biosensors [3], surfactants [4], and materials with enhanced properties [5] to name only a few examples. AFM can be employed in the analysis of forces such as adhesion [6,7] and friction [8,9] between surfaces of interest. The tips of AFM cantilevers can be modified through chemical functionalisation [10] or by the attachment of a colloidal particle such as silica [2,11,12].

The measurement of forces using AFM is a rapidly growing research area, and surface chemistry is often an important consideration during AFM adhesion force measurements [13] as the attractive or repulsive forces between two surfaces will be influenced by the chemistry of the surfaces. One particular area of interest is that of chemical force microscopy (CFM) measurements, where a surface and an AFM cantilever tip with well-defined surface chemistries are presented to each other, perhaps involving the modification of the AFM cantilever tip and the surface with self-assembled monolayers [10] CFM measurements are often made in aqueous environments [10] and typical variables are environmental ionic strength and pH, which can affect the adhesion between two surfaces by changing their ionisation state. Understanding the effect of surface chemistry on the interactions between surfaces in aqueous solution may impact upon research areas such as the development of microelectromechanical systems devices, biosensors, colloid science and drug development.

Upon their incorporation into the terminal moiety of a self-assembled monolayer (SAM), protonatable chemical species such as amines, carboxylic acids and phosphate groups have been shown to exhibit a shift in their pK_a when present at a surface, relative to their pK_a as measured in free solution [14–16]. This shift in pK_a has been attributed to the reduced availability and hindered orientation of the groups when present at the SAM surface. The use of contact angle measurements to estimate surface pK_as has previously been reported by Creager and Clarke [17] for mixed SAMs incorporating carboxylic acid-terminated alkanethiols. This work reports the synthesis of four disulfide species and the characterisation of the SAMs they form on Au thin films. Each SAM presents a surface pyridine or substituted pyridine moiety with a different predicted pK_a. The pK_as of the pyridine moieties were altered through the incorporation of fluorine, chlorine and bromine substituents in the pyridyl ring, providing a range of protonatable SAMs. The adhesive properties of the SAMs were investigated as a function of electrolyte pH and electrolyte concentration.

* Corresponding author. Tel.: +44 121 414 2739; fax: +44 121 414 5377.
E-mail address: k.kendall@bham.ac.uk (K. Kendall).

0040-6090/$ – see front matter © 2009 Published by Elsevier B.V.
doi:10.1016/j.tsf.2009.01.093

2. Experimental details

2.1. Chemical reagents

Four different dialkyl disulfides containing pyridine or substituted pyridine moieties were synthesised as described in Appendix A. The SAM structures, contact angle behaviour and the predicted pK_as (in aqueous solution) of their terminal pyridine moieties are listed in Table 1. Predictions were made using the Hammett and Taft equations for heteroaromatic acids and bases [18]. The organic solvents used for SAM formation were HPLC grade ethanol (EtOH, Fisher Scientific, UK) and analytical grade $CHCl_3$ (Fisher Scientific, UK). Piranha solution was used for glassware cleaning and for cleaning Au slides prior to SAM formation. Piranha solution was made as a 3:7 mixture of 30% laboratory reagent grade hydrogen peroxide (Fisher Scientific, UK) and analytical reagent grade concentrated sulfuric acid (Fisher Scientific, UK). Piranha solution is a very strong oxidising agent and has been known to detonate spontaneously upon contact with organic material. Therefore, eye protection (Fisher Scientific, UK) and nitrile gloves (Bodyguards, UK) were worn at all times, and as a precaution H_2O ice was used as a quenching agent.

When required for pH adjustments, NaOH solutions were made by dissolving NaOH pellets (Fisher Scientific, UK) in 18 MΩ ultra-high purity H_2O (Elga) at room temperature, followed by dilution as required. HCl solutions were made by diluting 11.65 M HCl solution (Fisher Scientific, UK) with 18 MΩ H_2O at room temperature. All pH measurements were performed using an IQ150 pH meter (IQ Scientific Instruments) operating at room temperature. A 150 mM phosphate-buffered saline (PBS) solution (pH 7.4) was prepared by dissolving a PBS tablet (Sigma, UK) in 18 MΩ H_2O (200 mL) at room temperature. The solution was adjusted to pH 3, 5, 7 and 9 through the addition of HCl solution or NaOH solution as necessary. A 0.1 mM PBS solution was prepared by diluting a 150 mM PBS solution with 18 MΩ H_2O. The 0.1 mM PBS solution was adjusted to pH 3, 5, 7 and 9 through the addition of HCl solution or NaOH solution as necessary. The ionic strengths of the adjusted 150 mM PBS solutions were all on the order of 200 mM, while the ionic strengths of the adjusted 0.1 mM PBS solutions were all on the order of 1–5 mM.

2.2. Deposition of Au thin films and formation of SAMs

Au was deposited onto clean glass microscope slides (BDH, UK) by thermal evaporation using an Auto 306 vacuum evaporation chamber (Edwards, UK), using Cr as an adhesion promoter. The chamber pressure was reduced to ~10^{-5} Pa using a two-stage pumping system. Cr pieces of 99.99% purity (Agar Scientific, UK) were heated by electrical resistance using a voltage of 30 V and a current of 3 A until ~5 nm of Cr had been deposited onto the glass surface. Au wire of 99.99+% purity (Advent Research Materials, UK) of 0.5 mm diameter was placed into a Mo boat (Agar Scientific, UK) and was heated by electrical resistance using a voltage of 10 V and a current of 3 A until ~100 nm of Au had been deposited onto the desired surface. Deposition was monitored using a quartz crystal microbalance (QCM) thickness monitor. The deposition rate for both Cr and Au was in the range 0.05–0.10 nm s^{-1}. Nitrile gloves (Bodyguards, UK) were worn during all handling procedures and Dumostar tweezers (Agar Scientific, UK) were employed to minimise contact with the samples whenever it was practical to do so. Where Au substrates were required to be cut up into smaller pieces, a diamond-tipped scriber (Agar Scientific, UK) was used. Any dust produced was blown away with Ar gas.

All glassware used in SAM formation was cleaned prior to use by immersion in piranha solution at room temperature for ~1 h. Cleaning with piranha solution was followed by rinsing with copious amounts of 18 MΩ H_2O (Elga) and drying in an oven at 140 °C. SAMs were prepared by immersing Cr-primed, Au-coated glass microscope slides in 1 mM solutions of the SAM compounds for 48 h, using either EtOH or $CHCl_3$ as a solvent. All Au substrates were cleaned prior to SAM formation by immersion in piranha solution at room temperature for 10 min. Cleaning with piranha solution was followed by rinsing with copious amounts of 18 MΩ H_2O (Elga) and rinsing with copious amounts of EtOH or $CHCl_3$, as was appropriate to the SAM solution solvent. After the desired immersion time, Au substrates were removed from the SAM solution and rinsed with copious amounts of either EtOH or $CHCl_3$, before being blown dry using Ar gas.

2.3. SAM characterisation and contact angle titration procedures

Characterisation of SAMs formed on Au substrates involved assessing their wetting behaviour, elemental composition and thickness, employing dynamic H_2O contact angle measurements, X-ray photoelectron spectroscopy and ellipsometry, respectively. Full descriptions of the SAM characterisation results can be found in the Appendix A. Dynamic H_2O contact angles were measured using a home-made stage apparatus, employing a Charge-Coupled Device (CCD) KP-M1E/K camera (Hitachi) and FTA Video Analysis software

Table 1
Chemical structures of SAM compounds 1–4, their H_2O contact angle behaviour and predicted pK_as in aqueous solution

SAM compound number	1	2	3	4
Compound structure	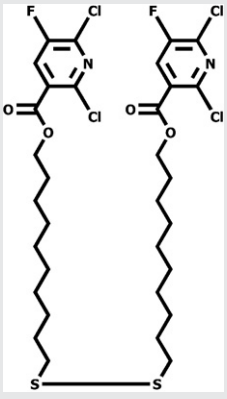	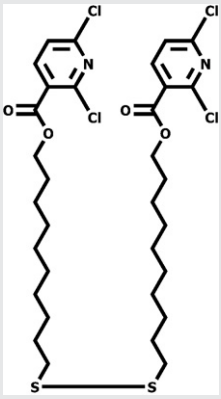	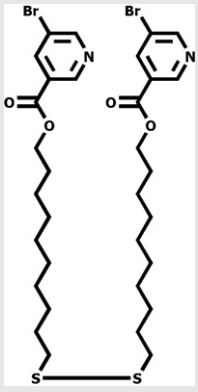	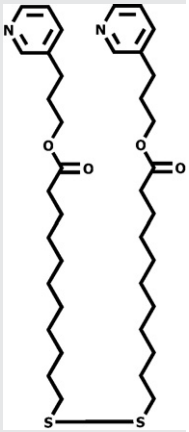
θ_a, H_2O (°)	88±2	92±1	91±1	54±2
θ_r, H_2O (°)	59±2	62±1	53±2	20±2
Predicted pK_a of pyridine moiety	−8.14	−6.14	0.88	5.60

Please cite this article as: J. Bowen, et al., Thin Solid Films (2009), doi:10.1016/j.tsf.2009.01.093

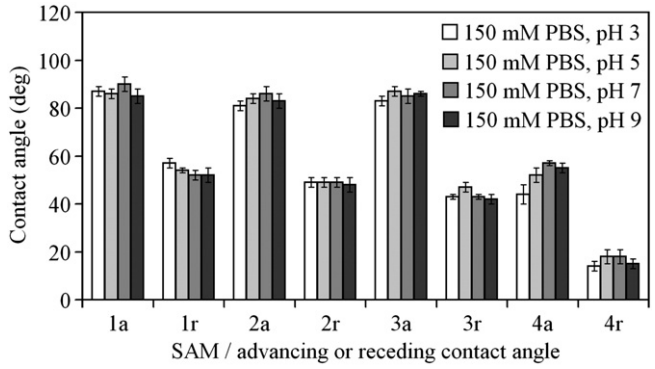

Fig. 1. Contact angle titration behaviour of SAMs 1–4 using 150 mM PBS at pH 3–9.

v1.96 (First Ten Angstroms) for analysis of the contact angle of a droplet of 18 MΩ H_2O at the three-phase intersection point. All data was collected at room temperature and pressure under ambient humidity conditions (approximately 50%). A 25 μL gastight syringe (Hamilton) was used for changing the volume of the droplet for all measurements, allowing volume adjustments of ~1 μL to be performed manually, if necessary. The droplet was released onto the sample surface from a blunt-ended needle of ~1 mm diameter (Hamilton). When measurements were performed with aqueous buffer solutions the same procedures were followed. All equipment was rinsed thoroughly with 18 MΩ H_2O after using aqueous buffer solutions. Frames for the video analysis were captured at a rate of 0.12 Hz, usually yielding a minimum of ten frames for both the advancing contact angle and the receding contact angle. Mathematical analysis of the contact angle was performed assuming a non-spherical droplet shape, with manual designation of the baseline for each surface analysed. Data for the advancing contact angle were only chosen when the droplet width was increasing. Similarly, data for the receding contact angle were only chosen when the droplet width was decreasing. The calculated contact angles for each frame during the advancing or receding droplet movement were averaged to give mean values for both the advancing and receding contact angle behaviour of the surface. A minimum of 7 measurements were performed for each sample.

Ellipsometry measurements were performed using a spectroscopic ellipsometer (Jobin-Yvon/Horiba, UK) operating with DeltaPsi2 v2.0.8 software. The angle of incidence was set to 70°. The wavelength range for the incident light was 280–800 nm. All measurements were made under conditions of ambient temperature, pressure and humidity. Mean film thicknesses were obtained from a minimum of six measurements at different locations on the substrate. Precautions were made to avoid performing measurements on visibly defective locations on the sample. Calculation of the SAM thickness was performed using a three-phase ambient/SAM/Au model, in which the SAM was assumed to be isotropic and assigned an initial refractive index of 1.50 [19–21]. The refractive index of a SAM has also been reported as 1.45 [22,23]. However, it was found that whether the starting value for the iterative calculation process was 1.45 or 1.50, the outcome of the modelling process did not vary. The SAM was modelled using a Cauchy transparent layer, whose initial thickness was varied using a multi-guess iterative calculation procedure.

XPS analysis of SAMs was performed using an Escalab 250 system (Thermo VG Scientific) operating with Avantage v1.85 software. An Al Kα X-ray source was used, providing a monochromatic X-ray beam with incident energy of 1486.68 eV. All measurements were made at a pressure of ~5×10^{-7} Pa. A circular spot size of ~0.2 mm^2 was employed throughout all measurements. Samples were immobilised onto stainless steel sample holders, using both double-sided carbon sticky tape (Shintron tape, Shinto Paint Company) and stainless steel or copper sample clips (Thermo VG Scientific). The use of clips provided conductivity between the sample surface and the sample holder, because although the Au film is conductive, the glass substrate is insulating. By providing a conductive link between the sample surface and the sample holder, surface charge retention during measurement was minimised. Low resolution survey spectra were obtained using a pass energy of 150 eV over a binding energy range of −10 eV to 1200 eV, obtained using 1 eV increments. Recorded low resolution spectra would typically be an average of 5 scans. All high resolution spectra were obtained using a pass energy of 20 eV over a binding energy range of 20–30 eV, centred around a chosen photoelectron binding energy, obtained using 0.1 eV increments. A dwell time of 20 ms was employed when collecting data from each binding energy increment for all measurements. Recorded high resolution spectra would typically be an average of at least 10 scans.

2.4. AFM adhesion force measurement procedure

AFM adhesion force measurements were performed using a MultiMode AFM (Veeco, UK) operating in a liquid environment. The MultiMode AFM operated an 'E' scanner, with a maximum lateral range of 14 μm×14 μm and a maximum vertical range of 3.8 μm. The AFM was housed on a vibration isolation table to minimise the effect of ambient noise on measurement quality. Nanoscope v5.12 software (Veeco, UK) was used throughout for both real-time analysis and post-capture results processing. Samples were immobilised onto steel SPM specimen disks (Agar Scientific, UK) using double-sided sticky tape (3 M, UK) prior to AFM analysis. All sample handling was carried out using Dumostar tweezers (Agar Scientific, UK) to minimise the risk of sample contamination.

A glass fluid cell (Veeco, UK) with a silicone O-ring (Veeco, UK) was employed for all force measurements. For each tip/sample/electrolyte combination, the electrolyte was housed in a 5 mL capacity Luer-Lok plastic syringe (Fisher Scientific, UK) prior to introducing the liquid to the fluid cell through clean silicone tubing (Veeco, UK). Prior to performing each measurement, the fluid cell was rinsed thoroughly with 18 MΩ H_2O and dried through absorption of H_2O using a small piece of paper towel (Kimberly Clark, UK). The fluid cell was subsequently irradiated with long-wave UV light (366 nm) for 20 min using a UV lamp (BDH, UK) positioned approximately 5 mm above the fluid cell. Upon being filled with electrolyte solution, the fluid cell was sealed off using tubing clips and the system was allowed to thermally equilibrate. Equilibration was deemed to have occurred once the vertical and horizontal deflection of the cantilever had stopped fluctuating.

Adhesion force measurements on SAMs were performed using triangular thick-legged Au-coated pyramidal-tipped Si_3N_4 cantilevers

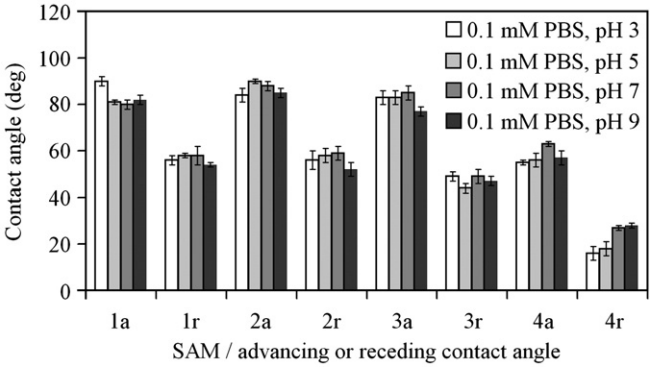

Fig. 2. Contact angle titration behaviour of SAMs 1–4 using 0.1 mM PBS at pH 3–9.

Please cite this article as: J. Bowen, et al., Thin Solid Films (2009), doi:10.1016/j.tsf.2009.01.093

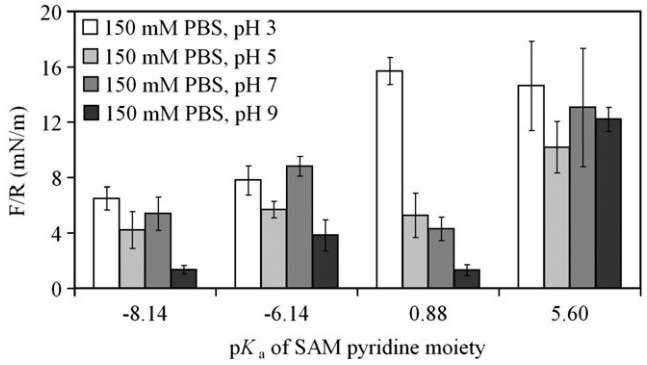

Fig. 3. Adhesion (jump-to) forces measured between the cantilever tip and SAMs 1–4 in 150 mM PBS at pH 3–9.

(Veeco, UK) with nominal spring constants of 0.12 N m^{-1} (200 μm length) and nominal tip radii of 30 nm. Data was acquired at tip velocities of 300–400 nm s^{-1}. Real-time 'Deflection–Separation' data was initially acquired for all measurements, displaying the motion of the cantilever relative to the separation distance between the cantilever tip and the surface. Upon completing the measurements, the data was processed to provide mean jump-to forces, which is the maximum force experienced by the cantilever tip upon its approach towards the SAM surface, for all tip/sample/electrolyte combinations.

3. Results and discussion

3.1. Contact angle titration behaviour of SAMs

Contact angle titration involves measuring the contact angle behaviour of a solid surface over a range of pH, generally performed using droplets of aqueous electrolyte adjusted to the desired pH. In this case, the contact angle behaviour of SAMs 1–4 was assessed using 150 mM and 0.1 mM PBS solutions adjusted to pH 3, 5, 7 and 9, affording analysis of the effect of pH and electrolyte concentration. The measured contact angle titration behaviour of SAMs 1–4 using 150 mM and 0.1 mM PBS solutions, shown in Figs. 1 and 2 respectively, reveal that the contact angle titration behaviour of SAMs 1–4 is similar to their contact angle behaviour measured using 18 MΩ H_2O. Furthermore, there is little variation in the contact angle behaviour of each SAM with either pH or electrolyte concentration. Interestingly, however, the contact angle behaviour of SAM 4 is 25–30° lower than the contact angle behaviour of SAMs 1–3. Such an effect could be attributable to the lower predicted pK_as of the terminal pyridine moieties of SAMs 1–3,−8.14,−6.14 and 0.88 respectively, as shown in Table 1, relative to that of SAM 1, which is 5.60, given the hydrophobic nature of the halogen substituents incorporated into their terminal moieties. As the pH range studied is lower than the predicted pK_as of the terminal pyridine moieties of SAMs 1–3, a change in contact angle behaviour would not reasonably be expected with pH. In comparison, as the pyridine moiety of SAM compound 4 has a predicted pK_a in aqueous solution of 5.60, a change in the protonation state of this moiety in the SAM formed from compound 4 between pH 5 and 7 might be expected, were the moiety present in free solution. However, the effect of surface confinement on the pK_a of the pyridine moieties appears to have altered the pK_a of these moieties such that a change in protonation state, and hence the contact angle behaviour of the SAM, does not occur between pH 5–7. The change in pK_a of moieties when present as the terminal moiety in SAMs has previously been reported for amino [14,15], carboxylic acid [16] and sulfonic acid [14] moieties, amongst others. Therefore, a change in the pK_a of the pyridine moieties of SAMs 1–4 could reasonably be expected here also. Inspection of the results for SAM 4 reveals no consistent trend in contact angle behaviour with pH for the two electrolyte concentrations studied. There is a slight decrease in contact angle behaviour for those measurements performed using 150 mM PBS solution between pH 3 and pH 5, but contact angle measurement is a relatively coarse method for examining subtle changes in surface character. Therefore, it is expected that the AFM force measurements will prove more sensitive to any change in the protonation state of the SAM terminal moieties. Interestingly, it has recently been reported that smoother Au surfaces produce greater shifts in the apparent surface pK_a of mercaptocarboxylic acid SAMs [24] and it may be that the roughness of the Au thin films employed here, which were found to have an R_a of 1 nm when imaged by AFM, has influenced the behaviour of these SAMs.

3.2. Adhesive properties of SAMs

AFM adhesion measurements were performed on SAMs 1–4 using a pyramidal-tipped Si_3N_4 AFM cantilever. Measurements were performed in 150 mM and 0.1 mM PBS solutions adjusted to pH 3, 5, 7 and 9. The jump-to forces exhibited by SAMs 1–4 measured in 150 mM and 0.1 mM PBS solutions are shown in Figs. 3 and 4 respectively. These results show that SAM 4 exhibited a greater jump-to force than SAMs 1–3, which all exhibited approximately similar jump-to forces. Therefore, the jump-to force as measured by AFM for each of the four SAMs follows the same trend as the contact angle behaviour, in that the SAMs with higher H_2O contact angle behaviour, and therefore less surface energy, exhibit smaller jump-to forces. It is interesting that the jump-to forces do not vary significantly with pH, which suggests that there is no electrostatic interaction occurring between SAM 4 and the AFM cantilever tip. Additionally, there is no significant change in the magnitude of the jump-to force between the two different electrolyte concentrations studied, which also suggests that the jump-to force is not electrostatic in nature. Upon the approach of the AFM cantilever tip to the SAMs in 0.1 mM PBS solution, but not in 150 mM PBS solution, a non-contact repulsive force was observed at pH 7 and pH 9 for all SAMs. The repulsive force, which did not vary significantly in magnitude between SAMs or with pH, probably occurred due to the increasing deprotonation of the SiO_2 surface of the AFM cantilever tip with increasing pH. It should be noted that the pull-off forces measured during the AFM measurements were approximately one order of magnitude greater than the measured jump-to forces, and displayed no apparent trend between SAMs or with pH and electrolyte concentration. The pull-off force is a result of a number of complex interactions at the AFM cantilever tip/SAM interface, with the possibility for rearrangement of SAM molecules and variations in contact area between tip and SAM, given the geometry of interaction in these systems. Indeed, given the large terminal moieties of SAMs 1 and 2, for example, there may be greater spacing between these molecules on the surface, allowing

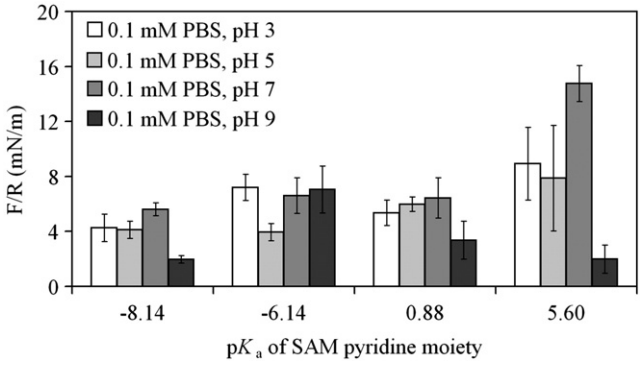

Fig. 4. Adhesion (jump-to) forces measured between the cantilever tip and SAMs 1–4 in 0.1 mM PBS at pH 3–9.

Please cite this article as: J. Bowen, et al., Thin Solid Films (2009), doi:10.1016/j.tsf.2009.01.093

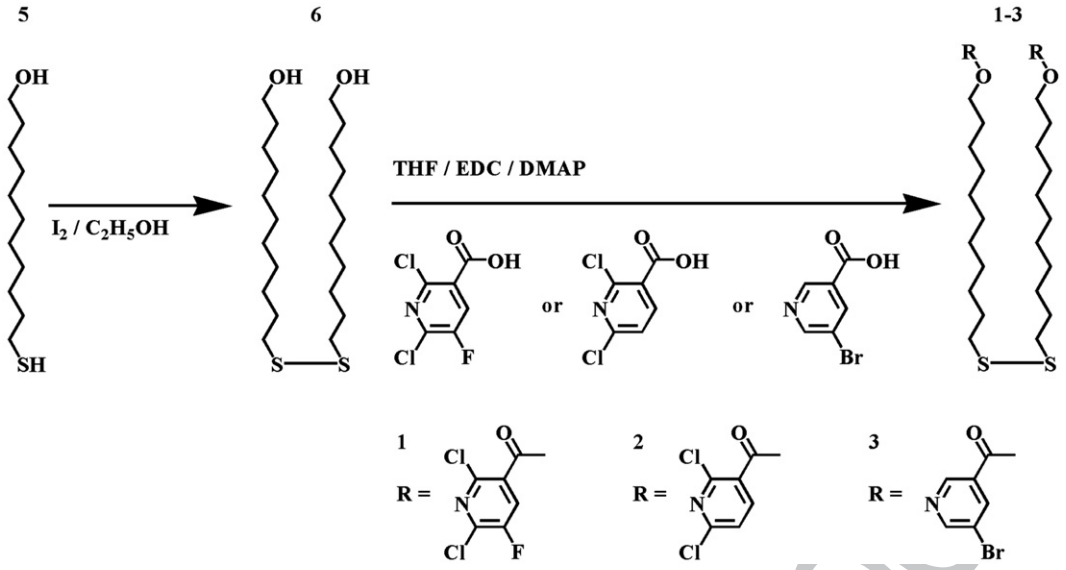

Scheme A1. Synthetic route employed for the synthesis of SAM compounds 1–3.

greater penetration of the AFM cantilever tip into the SAM, therefore increasing the contact area. Additionally, the roughness of the Au surface and the exact point of contact between the AFM cantilever tip and the SAM will also affect the results, as there will not be an idealised sphere-on-flat contact geometry at all locations. Fears et al. [25] recently described the analysis of the surface pK_as of COOH-and NH_2-terminated alkanethiols on Au surfaces using surface plasmon resonance (SPR), and this would seem to be a suitably sensitive technique with which to analyse the SAMs investigated here. SPR allows the solution pH local to the SAM surface to be analysed, at sub-nanometre resolution, and therefore the type and concentration of ion present adjacent to the SAM surface can be assessed, which would afford further insight into the protonation state of these pyridine-terminated SAMs.

4. Conclusions

The effect of electrolyte pH and electrolyte concentration on four pyridine-terminated SAMs has been investigated using contact angle titration and AFM adhesion measurements. Measurements performed either using or while immersed in 150 mM and 0.1 mM PBS solutions studied the adhesion behaviour of the SAMs. It was found that both the pH and concentration of the aqueous electrolyte have little effect on the contact angle titration behaviour and the adhesion force behaviour of the SAMs, with the exhibited forces being due to van der Waals forces, rather than electrostatic interactions between the tip and the SAM. Such behaviour suggests that the protonation state of the terminal pyridine moieties of the SAMs does not change over the pH range studied here, due to a shift in the pK_a of the pyridine moiety when present as the terminal group in a SAM. Similarly, the change in pK_a of amino [14,15], carboxylic acid [16] and sulfonic acid [14] moieties when present as the terminal moieties in SAMs has previously been reported. For the systems studied here, it does not appear that pK_a alone is a sufficient indicator of the adhesion behaviour of the system, whereas the presence of hydrophobic elements, such as the halogen substituents in the terminal moieties of SAMs 1–3, proved very influential on the results.

Acknowledgements

We acknowledge The University of Birmingham and ACORN (A Collaboration on Research into Nanoparticles) for financial support.

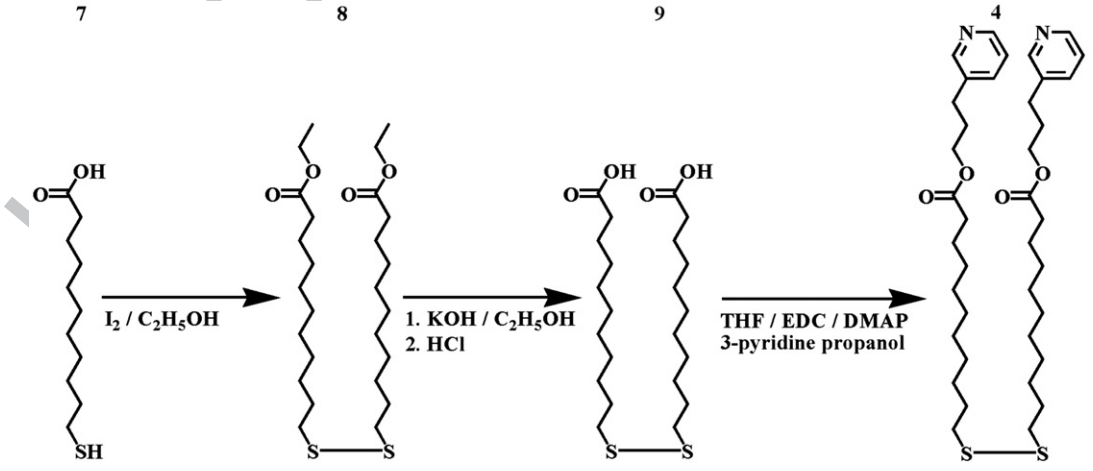

Scheme A2. Synthetic route employed for the synthesis of SAM compound 4.

Please cite this article as: J. Bowen, et al., Thin Solid Films (2009), doi:10.1016/j.tsf.2009.01.093

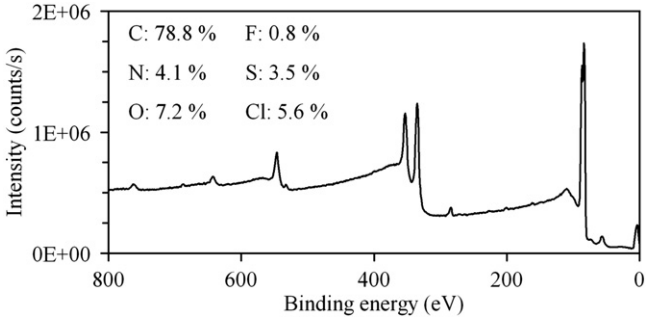

Fig. A1. XPS survey spectrum for SAM 1.

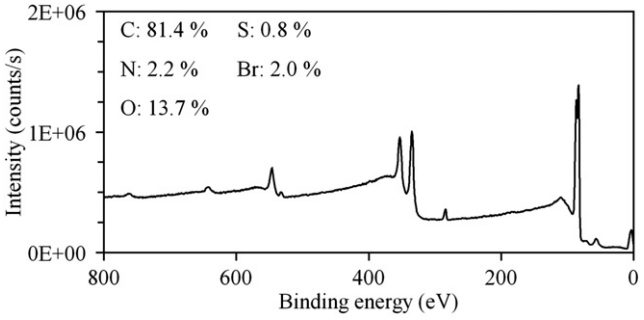

Fig. A3. XPS survey spectrum for SAM 3.

We also acknowledge the assistance for production of Cr-primed Au-coated glass microscope slides given by Professor G.J. Leggett and Dr. S. Sun at the University of Sheffield, School of Chemistry.

Appendix A

The following information is presented in the appendix. (i) Synthesis and characterisation data for SAM compounds 1–4. (ii) Characterisation results for SAMs 1–4, consisting of survey spectra and percentage elemental composition as determined by X-ray photoelectron spectroscopy, and thickness data as determined by ellipsometry.

A.1. Synthesis and characterisation data for SAM compounds 1–4

Schemes A1 and A2 show the synthetic route employed in order to obtain SAM compounds 1–4. Compounds 5–9 are the intermediates synthesized prior to obtaining SAM compounds 1–4, and all molecules are introduced in order of their synthesis beginning with the SAM compound with the simplest head group (4), with SAM compounds 1–4 having previously been numbered in the main text.

- Compound 8

To a solution of 11-mercaptoundecanoic acid 7 (7.0 g, 32.1 mM) in C_2H_5OH (100 mL) heated under reflux was added a solution of iodine (4.07 g, 16.03 mM) in C_2H_5OH (50 mL). Heating was continued for 12 h after which the reaction was allowed to cool to room temperature and washed with a saturated aqueous solution of $Na_2S_2O_3$ (50 mL). The products were extracted into CH_2Cl_2 (3×50 mL) and dried ($MgSO_4$), filtered and the solvent was removed *in vacuo*. The residues were purified by recrystallisation from CH_2Cl_2/hexane. The feathery white crystals were filtered from the mother liquor, washed with ice-cold hexane and dried *in vacuo* affording 8 (6.47 g, 82%). *m/z* (ES) 513 $[M+Na]^+$ δ_H (500 MHz, $(CD_3)_2SO$) 4.09 (4H, *q*, *J*=7.3, 14.3 Hz), 2.65 (4H, *t*, *J*=7.3 Hz), 2.26 (4H, *t*, *J*=7.3 Hz), 1.61 (8H, *m*), 1.34 (30H, *m*). δ_C (400 MHz, $CDCl_3$) 173.9, 60.1, 39.1, 34.4, 29.3, 29.2, 28.5, 24.9, 14.2. Elemental analysis of $C_{26}H_{50}O_4S_2$ requires C 63.67%, H 10.20%. Elemental analysis found C 63.52%, H 10.48%.

- Compound 9

To a vigorously stirred solution of 8 (4.75 g, 9.68 mM) in THF (100 mL) was added a solution of potassium hydroxide (1.63 g, 29.0 mM) in H_2O/C_2H_5OH (1:1, 20 mL). The reaction was stirred for 12 h, and acidified with HCl (aq, 2 M, 20 mL) upon which a white solid precipitated. The solid was filtered off, washed with H_2O (100 mL), cold C_2H_5OH (100 mL) and dried *in vacuo* affording 9 as white plate-like crystals (4.20 g, 99%). m/z (ES) 457 $[M+Na]^+$. δ_H (400 MHz $(CD_3)_2SO$) 3.5 (2H, s), 2.68 (4H, *t*, *J*=8.0 Hz), 2.14 (4H, *t*, *J*=8.0 Hz), 1.62 (4H, *m*), 1.46 (4H, *m*), 1.2 (24H,*m*). δ_C (400 MHz, $(CD_3)_2SO$) 174.5, 38.0, 33.7, 28.9, 28.8, 28.6, 28.6, 27.8, 24.5. Elemental analysis of $C_{22}H_{42}O_4S_2$ requires C 60.82%, H 9.67%. Elemental analysis found C 60.78%, H 9.70%.

- Compound 4

To a solution of 9 (0.100 g, 0.23 mM) in dry THF (10 mL) cooled to 0 °C under an N_2 atmosphere was added 1-(3-dimethylaminopropyl)-3-ethyl-carbodiimide hydrochloride (0.272 g, 1.38 mM) and a catalytic amount of 4-dimethyl-aminopyridine. The mixture was stirred for 30 min and 3-pyridinepropanol (0.094 g, 0.69 mM) was added over 10 min, followed by further stirring for 24 h under an N_2 atmosphere at room temperature. The white precipitate was filtered and the filtrate was diluted with CH_2Cl_2 (30 mL) and washed with H_2O (3×30 mL), followed by 10% aqueous $NaHCO_3$ (10 mL) and saturated (aqueous) NaCl (5 mL). The organic phase was dried ($MgSO_4$), filtered and the filtrate evaporated to dryness under reduced pressure. The residue was purified by silica gel column chromatography (eluent: CH_2Cl_2/EtOAc, 3:1) to yield 4 (0.045 g, 29%) as a white solid. *m/z* (ES) 695 $[M+Na]^+$. δ_H (400 MHz, $CDCl_3$) 8.4 (4H, *m*), 7.47 (2H, *m*), 7.19 (2H, *m*), 4.07 (4H, *t*, *J*=6.4 Hz), 2.66 (8H, *m*), 2.27 (4H, *t*, *J*=8.0 Hz), 1.94 (4H, *m*), 1.66 (8H, *m*), 1.32 (24H, *m*). δ_C (400 MHz, $CDCl_3$) 173.7, 149.9, 147.5, 136.3, 135.6,

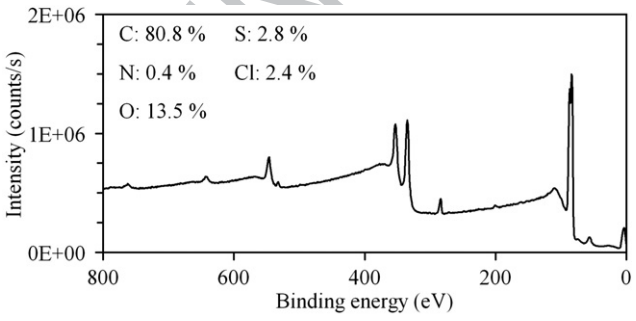

Fig. A2. XPS survey spectrum for SAM 2.

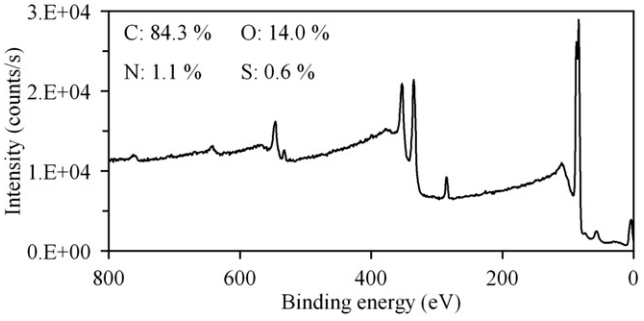

Fig. A4. XPS survey spectrum for SAM 4.

Table A1
Ellipsometrically measured thicknesses for SAMs 1–4

SAM	Calculated thickness range (nm)	Measured thickness (nm)
1	1.64–1.89	0.87±0.15
2	1.64–1.89	1.36±0.15
3	1.64–1.89	1.69±0.19
4	1.94–2.24	1.42±0.31

123.2, 63.1, 39.0, 34.2, 29.8, 29.3, 29.1, 28.4, 24.9. Elemental analysis of $C_{38}H_{60}O_4N_2S_2$ requires C 67.75%, H 8.91%, N 4.16%. Elemental analysis found C 67.80%, H 8.82%, N 4.07%.

- Compound 6
  The same procedure was followed as described for the preparation of compound 8, using 11-mercapto-1-undecanol 5 (1.0 g, 4.89 mM), and iodine (0.75 g, 2.94 mM) in C_2H_5OH (50 mL). This was yielded a white solid (600 mg, 61%). *m/z* (ES) 429 $[M+Na]^+$. δ_H (400 MHz, $CDCl_3$) 3.85 (4H, *t*, *J*=7.2 Hz), 2.58 (4H, *t*, *J*=6.9 Hz), 1.46 (4H, quintet, *J*=6.9 Hz), 1.56 (4H, *m*), 1.18–1.38 (28H, *m*). δ_C (400 MHz, CD_3OD) 63.1, 39.2, 32.8, 29.5, 29.5, 29.4, 29.2, 28.5, 25.7. Elemental analysis of $C_{22}H_{44}O_2S_2$ requires C 65.34%, H 10.89%. Elemental analysis found C 65.44%, H 10.83%.
- Compound 3
  The same procedure was followed as described for the preparation of compound 4, using 5-bromonicotinic acid (0.37 g,1.83 mM), compound 6 (0.25 g, 0.62 mM), EDC (0.71 g, 3.69 mM) in dry CH_2Cl_2 (25 mL). This yielded a white solid (150 mg, 31%). *m/z* (ES) 775 $[M+H]^+$. δ_H (400 MHz, $CDCl_3$) 8.38 (2H, *s*), 8.78 (2H, *s*), 9.28 (2H, *s*), 4.07 (4H, *t*, *J*=6.4 Hz) 2.27 (4H, *t*, *J*=8.0 Hz), 1.94 (4H, *m*), 1.66 (4H, *m*), 1.32 (28H, *m*). δ_C (400 MHz, $CDCl_3$) 163.9, 154.3, 148.7, 139.3, 127.6, 120.5, 70.0, 39.0, 29.3, 29.1, 28.5, 28.4, 25.8. Elemental analysis of $C_{34}H_{50}O_4N_2S_2Br_2$ requires C 52.70%, H 6.45%, N 3.61%. Elemental analysis found C 52.55%, H 6.39%, N 3.55%.
- Compound 1
  The same procedure was followed as described for the preparation of compound 4, using 2,6-dichloro-5-fluoro-3-pyridinecarboxylic acid (0.39 g, 1.85 mM), compound 6 (0.25 g, 0.62 mM), EDC (0.71 g, 3.69 mM) in dry CH_2Cl_2 (25 mL). This yielded a white solid (150 mg, 31%). *m/z* (ES) 790 [M]+. δ_H (400 MHz, $CDCl_3$) 7.98 (2H, *s*), 4.07 (4H, *t*, *J*=6.4 Hz) 2.27 (4H, *t*, *J*=8.0 Hz), 1.94 (4H, *m*), 1.66 (4H, *m*), 1.32 (28H, *m*). δ_H (400 MHz, $CDCl_3$) 162.6, 155.0, 152.2, 143.5, 140.6, 140.4, 128.5, 128.2, 126.8, 66.8, 39.1, 29.4, 29.2, 29.1, 28.5, 28.4, 26.0. Elemental analysis of $C_{34}H_{46}O_4N_2S_2Cl_4F_2$ requires C 51.77%, H 5.83%, N 3.55%. Elemental analysis found C 51.88%, H 6.03%, N 3.41%.
- Compound 2
  The same procedure was followed as described for the preparation of compound 4, using 2,6-dichloronicotinic acid (0.29 mg, 1.48 mM), compound 6 (0.20 g, 0.49 mM), EDC (0.57 g, 2.96 mM) in dry CH_2Cl_2 (25 mL). This yielded a white solid (150 mg, 41%). m/z (ES) 778 [M]+. δ_H (400 MHz, $CDCl_3$) 7.98 (4H, *d*, *J*=7.2 Hz), 4.07 (4H, *t*, *J*=6.4 Hz) 2.27 (4H, *t*, *J*=8.0 Hz), 1.94 (4H, *m*), 1.66 (4H, *m*), 1.32 (28H, *m*). δ_C (400 MHz, $CDCl_3$) 162.6, 151.3, 142.7, 122.5, 66.6, 39.0, 29.3, 29.1, 28.4, 25.8. Elemental analysis of $C_{34}H_{48}O_4N_2S_2Cl_4$ requires C 54.15%, H 6.36%, N 3.71%. Elemental analysis found C 53.80%, H 6.56%, N 3.30%.

A.2. Characterisation results for SAMs 1–4

- XPS
  Figs. A1–A4 show the survey spectra obtained for SAMs 1–4 respectively, as well as the percentage compositions of the SAM as calculated from XPS data. These results show that the SAMs all exhibited the correct element photoelectrons for the molecules from which the SAMs were formed. Additionally, no unexpected elements were found to be present in the SAMs, all of which suggests that the SAMs had formed successfully.
- Ellipsometry
  A thickness range for each SAM was calculated by estimating the length of the molecular structures of compounds 1–4 using ChemDraw Ultra (v7.0.1, CambridgeSoft, UK) and Chem3D Ultra (v7.0.0, CambridgeSoft, UK) software. The upper limit of the range is the full length of the SAM molecule. The chosen lower limit of the range is the height of the SAM molecule at a tilt angle of 30° to the surface normal. These values are given in Table A1. The results indicate that the SAMs had all formed, although their thicknesses tended to be lower than the lower value of the calculated thickness range, with the exception of SAM 3. Given that the SAM molecules all exhibit sterically bulky pyridine head groups, it is probable that the size of the head groups decreased the maximum achievable packing density of the molecules on the surface, leading to a lower than expected SAM thickness.

References

[1] G. Binnig, C.F. Quate, C. Gerber, Phys. Rev. Lett. 56 (1986) 930.
[2] W.A. Ducker, T.J. Senden, R.M. Pashley, Nature 353 (1991) 239.
[3] H-F. Ji, T. Thundat, Biosens. Bioelectron. 17 (2002) 337.
[4] J-F. Liu, G. Min, W.A. Ducker, Langmuir 17 (2001) 4895.
[5] G. Toikka, R.A. Hayes, J. Ralston, Colloid Surface A 141 (1998) 3.
[6] M. Giesbers, J.M. Kleijn, M.A.C. Stuart, J. Colloid Interface Sci. 252 (2002) 138.
[7] M. Kappl, H-J. Butt, Part. Part. Syst. Charact. 19 (2002) 129.
[8] A. Lio, C. Morant, D.F. Ogletree, M. Salmeron, J. Phys. Chem. B. 101 (1997) 4767.
[9] N.J. Brewer, B.D. Beake, G.J. Leggett, Langmuir 17 (2001) 1970.
[10] A. Noy, D.V. Vezenov, C.M. Lieber, Annu. Rev. Mater. Sci. 27 (1997) 381.
[11] W.R. Bowen, N. Hilal, R.W. Lovitt, C. Wright, J. Colloid Surfaces A 157 (1999) 117.
[12] W.A. Ducker, T.J. Senden, R.M. Pashley, Langmuir 8 (1992) 1831.
[13] T.J. Senden, Curr. Opin. Colloid Interface Sci. 6 (2001) 95.
[14] B. Wang, R.D. Oleschuk, J.H. Horton, Langmuir 21 (2005) 1290.
[15] M.L. Wallwork, D.A. Smith, J. Zhang, J. Kirkham, C. Robinson, Langmuir 17 (2001) 1126.
[16] D.A. Smith, M.L. Wallwork, J. Zhang, J. Kirkham, C. Robinson, A. Marsh, M. Wong, J. Phys. Chem. B 104 (2000) 8862.
[17] S.E. Creager, J. Clarke, Langmuir 10 (1994) 3675.
[18] D.D. Perrin, B. Dempsey, E.P. Serjeant, pK_a Prediction for Organic Acids and Bases, Chapman and Hall, London, 1981.
[19] M.D. Porter, T.B. Bright, D.L. Allara, C.E.D. Chidsey, J. Am. Chem. Soc. 109 (1987) 3559.
[20] C.D. Bain, E.B. Troughton, Y-T. Tao, J. Evall, G.M. Whitesides, R.G. Nuzzo, J. Am. Chem. Soc. 111 (1989) 321.
[21] S.D. Evans, R. Sharma, A. Ulman, Langmuir 7 (1991) 156.
[22] H.A. Biebuyck, C.D. Bain, G.M. Whitesides, Langmuir 10 (1994) 1825.
[23] R. Colorado Jr., R.J. Villazana, T.R. Lee, Langmuir 14 (1998) 6337.
[24] S.C. Burris, Y. Zhou, W.A. Maupin, A.J. Ebelhar, M.W. Daugherty, J. Phys. Chem. C 112 (2008) 6811.
[25] K.P. Fears, S.E. Creager, R.A. Latour, Langmuir 24 (2008) 837.

Please cite this article as: J. Bowen, et al., Thin Solid Films (2009), doi:10.1016/j.tsf.2009.01.093